Dalton Transactions

PAPER

View Article Online
View Journal | View Issue

Cite this: *Dalton Trans.*, 2016, **45**, 15427

Octahedral molybdenum cluster complexes with aromatic sulfonate ligands†

Olga A. Efremova,*[a,b] Yuri A. Vorotnikov,[c] Konstantin A. Brylev,[c,d] Natalya A. Vorotnikova,[c] Igor N. Novozhilov,[c] Natalia V. Kuratieva,[c,d] Mariya V. Edeleva,[e] David M. Benoit,[a] Noboru Kitamura,[f] Yuri V. Mironov,[c,d] Michael A. Shestopalov*[c,d] and Andrew J. Sutherland[b]

Received 19th July 2016,
Accepted 30th August 2016

DOI: 10.1039/c6dt02863b

www.rsc.org/dalton

This article describes the synthesis, structures and systematic study of the spectroscopic and redox properties of a series of octahedral molybdenum metal cluster complexes with aromatic sulfonate ligands $(^nBu_4N)_2[\{Mo_6X_8\}(OTs)_6]$ and $(^nBu_4N)_2[\{Mo_6X_8\}(PhSO_3)_6]$ (where X^- is Cl^-, Br^- or I^-; OTs^- is *p*-toluenesulfonate and $PhSO_3^-$ is benzenesulfonate). All the complexes demonstrated photoluminescence in the red region and an ability to generate singlet oxygen. Notably, the highest quantum yields (>0.6) and narrowest emission bands were found for complexes with a $\{Mo_6I_8\}^{4+}$ cluster core. Moreover, cyclic voltammetric studies revealed that $(^nBu_4N)_2[\{Mo_6X_8\}(OTs)_6]$ and $(^nBu_4N)_2[\{Mo_6X_8\}(PhSO_3)_6]$ confer enhanced stability towards electrochemical oxidation relative to corresponding starting complexes $(^nBu_4N)_2[\{Mo_6X_8\}X_6]$.

Introduction

Octahedral molybdenum cluster complexes of the general formula $[\{Mo_6X_8\}L_6]$ (where X^- are inner halide ligands and L are apical organic or inorganic ligands) have been known for several decades since the structure, luminescence and redox properties of the $[\{Mo_6Cl_8\}Cl_6]^{2-}$ anionic unit were established and studied comprehensively.[1–8] However, in the last decade there has been a resurgence of interest in related octahedral molybdenum complexes. This is due to recent reports detailing the outstanding photoluminescence properties of some molybdenum octahedral cluster complexes. In general, these studies showed that upon UV-visible excitation cluster complexes based on a $\{Mo_6X_8\}^{4+}$ core demonstrated emission in both the red and near-infrared regions with high quantum yields and photoluminescence lifetimes of up to several hundreds of microseconds.[9–15] Moreover, these cluster complexes also demonstrated the capability to generate singlet oxygen efficiently.[13–16] These photoemissive properties combined with the relative chemical robustness of the $\{Mo_6X_8\}^{4+}$ cluster core make such complexes excellent candidates for photonic (*e.g.* materials for lasers[17] and optical waveguides[18]), photovoltaic,[19] biological and medical (*e.g.* imaging agents,[20,21] bactericides,[22] photo-dynamic therapy[23,24]) and environmental protection (*e.g.* hazardous organic waste decomposition[25,26]) applications.

It was shown recently that complexes with a $\{Mo_6I_8\}^{4+}$ cluster core ligated by residues of some strong oxoacids – either organic (fluorinated aliphatic acids[9,13]) or inorganic acids (nitric acid[11,27]) – demonstrated outstanding photophysical properties in comparison with those based on a $\{Mo_6Cl_8\}^{4+}$ or $\{Mo_6Br_8\}^{4+}$ core. These include not only significantly higher photoluminescence quantum yields at ambient conditions, but also comparatively narrow emission spectra profiles.

Therefore, we were keen to understand whether the same tendency in photophysical properties of $\{Mo_6X_8\}^{4+}$ cluster complexes is retained in cases, when they are coordinated by sulfonate aromatic outer ligands that are also anions of strong acids. Accordingly, we report the synthesis and systematic study of the photophysical and electrochemical properties of molybdenum cluster complexes $(^nBu_4N)_2[\{Mo_6X_8\}L_6]$, where L^- = *p*-toluenesulfonate (OTs^-) and X^- = Cl^- (**1**) Br^- (**2**) or I^- (**3**) or L = benzenesulfonate ($PhSO_3^-$) and X^- = Cl^- (**4**), Br^- (**5**) or I^- (**6**).

[a]*Department of Chemistry, University of Hull, Cottingham Road, Hull, HU6 7RX, UK. E-mail: o.efremova@hull.ac.uk*
[b]*Aston Materials Centre, Aston University, Aston Triangle, Birmingham, B4 7ET, UK*
[c]*Nikolaev Institute of Inorganic Chemistry SB RAS, 3 Acad. Lavrentiev Ave., 630090 Novosibirsk, Russian Federation*
[d]*Novosibirsk State University, 2 Pirogova Str., 630090 Novosibirsk, Russian Federation*
[e]*Novosibirsk Institute of Organic Chemistry SB RAS, 9 Acad. Lavrentiev ave., 630090 Novosibirsk, Russian Federation*
[f]*Department of Chemistry, Faculty of Science, Hokkaido University, 060-0810 Sapporo, Japan*

†Electronic supplementary information (ESI) available: DFT calculations data, single crystal data; singlet oxygen-generation data; examples of NMR spectra; cyclic voltammograms; the Tauc plot of the absorption spectra of $(^nBu_4N)_2[\{Mo_6X_8\}X_6]$; average values of the important bond lengths and angles. CCDC 1425980–1425985. For ESI and crystallographic data in CIF or other electronic format see DOI: 10.1039/c6dt02863b

Experimental section

Materials

$Cs_2[\{Mo_6X_8\}X_6]$,[28,29] $(^nBu_4N)_2[\{Mo_6X_8\}X_6]$,[30–32] silver benzenesulfonate[33] and 2,3-diphenyl-*p*-dioxene[34] were synthesised according to previously reported procedures. All other reactants and solvents were purchased from Fisher, Alfa Aesar and Sigma-Aldrich and used as received.

Instrumentation

NMR spectra of **1–6** were recorded on a Bruker Avance 300 NMR spectrometer equipped with a solution-state dual channel probe working at 300.13 MHz for ^{1}H and 75 MHz for ^{13}C. NMR spectra were measured in $CDCl_3$ or in acetone-d_6 in the standard way using the zg30 pulse program for ^{1}H. Elemental analyses were obtained using a EuroVector EA3000 Elemental Analyser. FTIR spectra were recorded on a Bruker Vertex 80 as KBr disks. Absorption spectra were recorded on a PerkinElmer Lambda35 UV-vis spectrometer.

Cyclic voltammetry

Cyclic voltammetry (CV) was performed using a Metrohm 797 VA Computrace instrument with a glassy carbon electrode as the working electrode and a saturated silver/silver chloride (Ag/AgCl) in 3.5 M KCl as a reference electrode, against which the half-wave potential of the ferrocene/ferrocenium (Fc/Fc^+) redox couple ($E_{1/2}$, Fc/Fc^+) was found to be 0.598 V. The potentials were related to the standard platinum electrode. A 0.15 M solution of tetra-*n*-butylammonium perchlorate ($^nBu_4NClO_4$) in acetonitrile was used as the electrolyte. Solutions of the samples in the electrolyte (1–2 mM) were degassed by purging with argon prior to recording the CV measurements. Compounds **1–6** as well as starting compounds $(^nBu_4N)_2[\{Mo_6X_8\}X_6]$ (X^- = Cl^-, Br^-, I^-) were investigated voltammetrically within the potential window from −2 V to 2.3 V at 25 °C. The formal half-wave potentials ($E_{1/2}$) were calculated as the midpoint between the anodic and cathodic peak potentials of the first oxidation of the cluster complex.

Photoluminescence measurements

For photoluminescence measurements, powdered samples of the complexes were placed between two non-fluorescent glass plates. The absorbance of acetonitrile solutions was set at <0.1 at 355 nm. The solutions were poured into quartz cuvettes. To deaerate, the solutions were purged with an Ar-gas stream for 30 min and then the cuvettes were sealed. Measurements were carried out at 298 K. The samples were excited by 355 nm laser pulses (6 ns duration, LOTIS TII, LS-2137/3). Corrected emission spectra were recorded on a red-light-sensitive multichannel photodetector (Hamamatsu Photonics, PMA-11). For emission decay measurements, the emission was analysed using a streakscope system (Hamamatsu Photonics, C4334 and C5094). The emission quantum yields were determined using an Absolute Photo-Luminescence Quantum Yield Measurement System (Hamamatsu Photonics, C9920-03), which comprised a xenon excitation light source (the excitation wavelength was set at 400 nm), an integrating sphere, and a red-sensitive multichannel photodetector (Hamamatsu Photonics, PMA-12).

Synthesis

General procedure for synthesis of $(^nBu_4N)_2[\{Mo_6X_8\}L_6]$ (L = OTs^-, X^- = Cl^- (1), Br^- (2) or I^- (3); L^- = $PhSO_3^-$, X^- = Cl^- (4), Br^- (5) or I^- (6)). 100 mg of $(^nBu_4N)_2[\{Mo_6X_8\}X_6]$ (0.064 mmol for X^- = Cl^-, 0.046 mmol for X^- = Br^-, 0.035 mmol for X^- = I^-) and 6.1 equiv. of AgOTs or $C_6H_5SO_3Ag$ were dissolved in 20 mL of acetone. The reaction mixture was stirred for 5 days at room temperature in a flask covered by aluminum foil. The precipitates of AgX were sedimented by centrifugation (7000 rpm, 5 min). The supernatant was decanted and the solvent evaporated on a rotary evaporator. The resultant solid residue was dissolved in 2 mL of acetone. The products were precipitated by adding 20 mL of diethyl ether and collected by filtration. To obtain single crystals for XRD the acetone solutions were subjected to slow diffusion of diethyl ether vapour.

1: Yellow. Yield: 130 mg (86%). Anal. calcd for $C_{74}H_{114}Cl_8Mo_6N_2O_{18}S_6$: C 37.5, H 4.8, N 1.2, S 8.1; found: C 37.5, H 4.8, N 1.2, S 8.4. UV-vis (CH_2Cl_2): λ_{max}, nm (ε, M^{-1} cm^{-1}) = 350 (sh, 3.2×10^3). FTIR (KBr, cm^{-1}): $\nu_{as}(SO_2)$ – 1295s, 1283s; $\nu_s(SO_2)$ – 1159s; ν(SO) – 958. ^{1}H NMR (acetone-d_6) δ (ppm): 7.67 [12H, d, $6 \times 2H^{ortho}$], 7.29 [12H, d, $6 \times 2H^{meta}$], 3.43 [16H, t, $2 \times 4CH_2$], 2.39 [18H, s, $6 \times CH_3$], 1.81 [16H, quin, $2 \times 4CH_2$], 1.43 [16H, sex, $2 \times 4CH_2$], 0.97 [24H, t, $2 \times 4CH_3$].

2: Yellow. Yield: 112 mg (90%) Anal. calcd for $C_{74}H_{114}Br_8Mo_6N_2O_{18}S_6$: C 32.6, H 4.2, N 1.0, S 7.1; found: C 32.6, H 4.2, N 1.0, S 6.8. UV-vis (CH_2Cl_2): λ_{max}, nm (ε, M^{-1} cm^{-1}) = 320 (5.0×10^3), 363 (sh, 3.4×10^3). FTIR (KBr, cm^{-1}): $\nu_{as}(SO_2)$ – 1293s, 1277s; $\nu_s(SO_2)$ – 1158s; ν(SO) – 964. ^{1}H NMR (acetone-d_6) δ: 7.64 [12H, d, $6 \times 2H^{ortho}$], 7.28 [12H, d, $6 \times 2H^{meta}$], 3.44 [16H, t, $2 \times 4CH_2$], 2.39 [18H, s, $6 \times CH_3$], 1.81 [16H, quin, $2 \times 4CH_2$], 1.43 [16H, sex, $2 \times 4CH_2$], 0.97 [24H, t, $2 \times 4CH_3$].

3: Orange. Yield: 95 mg (87%) Anal. calcd for $C_{74}H_{114}I_8Mo_6N_2O_{18}S_6$: C 28.6, H 3.7, N 0.9, S 6.2; found: C 28.7, H 3.6, N 0.9, S 6.0. UV-vis (CH_2Cl_2): λ_{max}, nm (ε, M^{-1} cm^{-1}) = 347 (5.2×10^3), 394 (4.3×10^3). FTIR (KBr, cm^{-1}): $\nu_{as}(SO_2)$ – 1269s; $\nu_s(SO_2)$ – 1157s; ν(SO) – 982. ^{1}H NMR (acetone-d_6) δ: 7.59 [12H, d, $6 \times 2H^{ortho}$], 7.27 [12H, d, $6 \times 2H^{meta}$], 3.43 [16H, t, $2 \times 4CH_2$], 2.39 [18H, s, $6CH_3$], 1.81 [16H, quin, $2 \times 4CH_2$], 1.43 [16H, sex, $2 \times 4CH_2$], 0.97 [24H, t, $2 \times 4CH_3$].

4: Yellow. Yield: 101 mg (67%). Anal. calcd for $C_{68}H_{102}Cl_8Mo_6N_2O_{18}S_6$: C 35.7, H 4.5, N 1.2, S 8.4; found: C 35.7, H 4.5, N 1.3, S 8.1. UV-vis (CH_2Cl_2): λ_{max}, nm (ε, M^{-1} cm^{-1}) = 348 (sh, 3.5×10^3). FTIR (KBr, cm^{-1}): $\nu_{as}(SO_2)$ – 1298s, 1285s; $\nu_s(SO_2)$ – 1161s; ν(SO) – 957. ^{1}H NMR (acetone-d_6) δ: 7.85–7.72 [12H, m, $6 \times 2H^{ortho}$], 7.54–7.41 [18H, m, $6 \times (2H^{meta} + H^{para})$], 3.43 [16H, t, $2 \times 4CH_2$], 1.80 [16H, quin, $2 \times 4CH_2$], 1.42 [16H, sex, $2 \times 4CH_2$], 0.96 [24H, t, $2 \times 4CH_3$].

5: Yellow. Yield: 90 mg (72%) Anal. calcd for $C_{68}H_{102}Br_8Mo_6N_2O_{18}S_6$: C 30.9, H 3.9, N 1.1, S 7.3; found: C 30.6, H 3.7, N 1.0, S 7.6 UV-vis (CH_2Cl_2): λ_{max}, nm

(ε, M^{-1} cm^{-1}) = 317 (5.2×10^3), 367 (3.6×10^3). FTIR (KBr, cm^{-1}): $\nu_{as}(SO_2)$ – 1282s; $\nu_s(SO_2)$ – 1162s; ν(SO) – 965. ^{1}H NMR (acetone-d_6) δ: 7.80–7.71 [12H, m, 6 × $2H^{ortho}$], 7.55–7.41 [18H, m, 6 × ($2H^{meta}$ + H^{para})], 3.43 [16H, t, 2 × $4CH_2$], 1.80 [16H, quin, 2 × $4CH_2$], 1.43 [16H, sex, 2 × $4CH_2$], 0.98 [24H, t, 2 × $4CH_3$].

6: Orange. Yield: 94 mg (87%). Anal. calcd for $C_{68}H_{102}I_8Mo_6N_2O_{18}S_6$: C 27.1, H 3.4, N 0.9, S 6.4; found: C 27.4, H 3.3, N 0.9, S 6.2. UV-vis (CH_2Cl_2): λ_{max}, nm (ε, M^{-1} cm^{-1}) = 347 (5.8×10^3), 391 (4.7×10^3). FTIR (KBr, cm^{-1}): $\nu_{as}(SO_2)$ – 1272s; $\nu_s(SO_2)$ – 1156s; ν(SO) – 985. ^{1}H NMR (acetone-d_6) δ: 7.75–7.67 [12H, m, 6 × $2H^{ortho}$], 7.52–7.43 [18H, m, 6 × ($2H^{meta}$ + H^{para})], 3.43 [16H, t, 2 × $4CH_2$], 1.81 [16H, quin, 2 × $4CH_2$], 1.43 [16H, sex, 2 × $4CH_2$], 0.97 [24H, t, 2 × $4CH_3$].

Crystal structure determination

Single-crystal X-ray diffraction data were collected at 150 K on a Bruker Nonius X8 Apex 4 K CCD diffractometer fitted with graphite monochromatised MoKα radiation (λ = 0.71073 Å). All crystallographic information is summarised in Table 1S.† Absorption corrections were made empirically using the SADABS program.[35] The structures were solved by the direct method and further refined by the full-matrix least-squares method using the SHELXTL program package.[35] All non-hydrogen atoms were refined anisotropically. The positions of the hydrogen atoms of the tetra-*n*-butylammonium cation, organic ligands and solvent molecules, apart from water molecules, were calculated corresponding to their geometrical conditions and refined using the riding model. The positions of hydrogen atoms for water molecules weren't localised. In the crystal structures of **2–4** and **6** the disorder of sulfonate groups was caused by the rotation of terminal groups around the C–S, S–O or Mo–O bonds.

CCDC 1425980–1425985 contain the supplementary crystallographic data for this paper.

Singlet oxygen generation

The ability of **1–6** to generate singlet oxygen was investigated semi-quantitatively as follows: 0.6 mL of an acetone-d_6 solution containing 0.0012 mmol of a cluster complex analyte and 0.12 mmol of the singlet oxygen trap molecule 2,3-diphenyl-*p*-dioxene[36,37] was placed in a conventional NMR tube and purged with oxygen gas for 5 min. The tube was sealed and then irradiated using filtered light ($\lambda \geq 400$ nm) from a DRSh-500 mercury lamp. ^{1}H NMR (200 MHz) spectra were recorded on a Bruker Avance 200 NMR spectrometer after 0, 1, 3 and 5 h of irradiation. The conversion of the trap molecule was calculated as a ratio of the aliphatic hydrogen peak integral of the oxidation product of 2,3-diphenyl-*p*-dioxene, namely ethylene glycol dibenzoate, to the sum of the integrals of the aliphatic hydrogen peaks of 2,3-diphenyl-*p*-dioxene and the oxidation product, ethylene glycol dibenzoate (see Fig. 1S and 2S†).

Results and discussion

Synthesis and characterization of $(^nBu_4N)_2[\{Mo_6X_8\}L_6]$ (L = OTs^-, X^- = Cl^- (1), Br^- (2) or I^- (3); L^- = $PhSO_3^-$, X^- = Cl^- (4), Br^- (5) or I^- (6))

To obtain $(^nBu_4N)_2[\{Mo_6X_8\}L_6]$ we used a well-established approach, in which tetra-*n*-butylammonium salts of molybdenum halide anions $[\{Mo_6X_8\}X_6]^{2-}$ (X^- = Cl^-, Br^- or I^-) were allowed to react with a silver salt of the corresponding sulfonic acid – either *p*-toluenesulfonic acid (HOTs) or benzenesulfonic acid ($PhSO_3H$). In these reactions – driven to completion by the formation of poorly-soluble and thermodynamically favourable silver halides – only the terminal halides were substituted by anionic ligands.[9–15,38–42] In all cases the reactions proceeded smoothly and resulted in the formation of $(^nBu_4N)_2[\{Mo_6X_8\}(OTs)_6]$ (X^- = Cl^- (**1**), Br^- (**2**), I^- (**3**)) and $(^nBu_4N)_2[\{Mo_6X_8\}(PhSO_3)_6]$ (X^- = Cl^- (**4**), Br^- (**5**), I^- (**6**)), respectively. The purity of compounds **1–6** was confirmed by both elemental analysis and NMR spectroscopy.

As expected, due to the symmetry of the cluster anions, only one set of signals, associated with the organic ligands, was observed in the ^{1}H NMR, with the ratio of signals from $^nBu_4N^+$ and the organic ligands being 1 : 3 (Fig. 3S†). Moreover, in each case the good agreement of the elemental analysis data with the theoretically calculated formula also supports the proposed compositions of the compounds synthesised.

It should be mentioned that the above reaction, although conducted in a different solvent (CH_2Cl_2 instead of acetone), has been used previously to synthesise **1**.[39,41] While Johnston *et al.* did not succeed in the structural characterization of the complex, Sokolov *et al.*[41] obtained crystals of solvates **1**·$2CH_2Cl_2$ (space group *Pbca*) and **1**·$2CH_3CN$ (space group $P2_1/c$) by slow diffusion of diethyl ether vapour into either a CH_2Cl_2 or an acetonitrile solution of **1** respectively.

We crystallised **1–6** by slow diffusion of diethyl ether vapour into acetone solutions to generate crystals suitable for characterisation by single crystal XRD. The crystallographic data obtained are summarised in Table 1S.† In our case, all six complexes crystallised in the triclinic ($P\bar{1}$) crystal system. It is clear that the choice of solvent resulted in crystals of **1** attaining a different space group from those published previously.[41] Moreover, in our work, crystals of compound **1** did not contain any solvate molecules. Indeed, only compounds **2** and **3** crystallised as solvates: with acetone, diethyl ether and water (**2**) or acetone and water (**3**).

Although compounds **1–3** and **4–6** are cluster complexes of very similar compositions, only crystals of pairs of compounds **2** and **3**, and **4** and **5** have similar crystal structures. In the independent part of the crystal structures of **2–5** there are two halves of the cluster anions $[\{Mo_6X_8\}L_6]^{2-}$ and two $^nBu_4N^+$ cations, while compounds **1** and **6** have only a half of the corresponding cluster anion and a $^nBu_4N^+$ cation in the independent part. In all cases the centre of the $[\{Mo_6X_8\}L_6]^{2-}$ cluster anion coincides with the inversion centre.

Similar to other octahedral molybdenum cluster complexes, the Mo_6 octahedra in compounds **1–6** are coordinated by eight

μ_3-type halide ligands and, additionally, each molybdenum is coordinated by a terminal ligand – *p*-toluenesulfonate or benzenesulfonate ion. The organic ligands are coordinated in a monodentate mode *via* an oxygen atom of the SO_3 group, as shown in Fig. 1. The important average bond lengths and angles in the crystal structures of compounds **1–6** are summarised in Table 2S.† The average bond lengths Mo–O are between 2.100–2.165 Å and they tend to increase with increasing size of the cluster core. Analysis of the Cambridge Structural Database (CSD)[43] data on the typical Mo–OSO_2 bond values show that the values found for **1–6** are towards the shorter range of these bond lengths. This observation indicates significant covalent contribution in the bonding. The Mo–O–S bond angles also tend to increase (*i.e.* deviate more significantly from the ideal tetrahedral bond angle) with increasing size of the cluster core, with the highest values, 140.6° and 142.1°, found in structures **3** and **6**, respectively. These values are slightly higher than the most typical bond angles between sulfonate groups and molybdenum atoms (128–138° according to CSD).

The FTIR spectra of compounds **1–6** are very similar, as bands originate mostly from the organic ligands and ^{n}Bu$_4$N$^+$ cations. The strong vibrations in the sulfonate group (Fig. 2) provide a simple way of monitoring the coordination of sulfonate ligands to the metal centres. Namely, the FTIR spectra of **1–6** further confirm the mono-dentate coordination mode of sulfonate groups. In comparison with the $\nu(SO_2)$ bands observed in the FTIR spectra of *p*-toluenesulfonic acid and benzenesulfonic acid $\nu(SO_2)$ bands observed in spectra of the obtained molybdenum cluster complexes are downshifted.[44,45] Moreover, minor changes are noticeable when comparing FTIR spectra of complexes with the same ligands, but different halide ligands in the cluster core (Fig. 2). Specifically, in the series Cl–Br–I there is a noticeable upshift of ν(S–O) bands especially in case of compounds **3** and **6**. This shift might indicate the change of the force constants (*i.e.* bonding order) for the S–O bonds, which can be additional evidence of some increase of the ionicity of the bonding between sulfonate groups and the molybdenum atoms. The DFT calculations undertaken for the crystal structures of **1–6** did not however confirm significant changes in the ionic nature of the bonding between the SO_3^- groups and the Mo cluster core (see ESI for details of DFT calculations, Table 3S†).

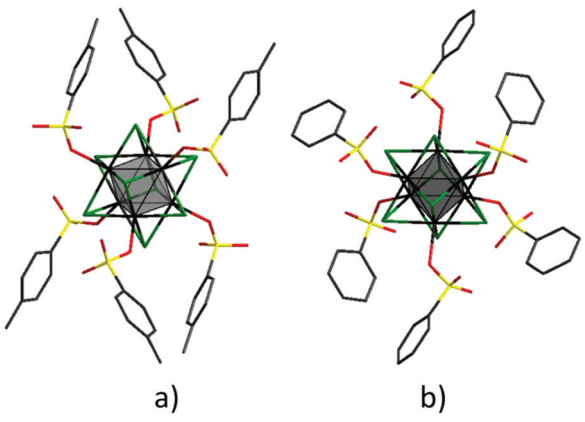

Fig. 1 The structure of the cluster anions $[\{Mo_6X_8\}(OTs)_6]^{2-}$ (a) and $[\{Mo_6X_8\}(PhSO_3)_6]^{2-}$ (b), where X^- = Cl^-, Br^- or I^-: Mo – black; X – green; S – yellow; O – red; C – charcoal; hydrogen atoms are omitted for clarity.

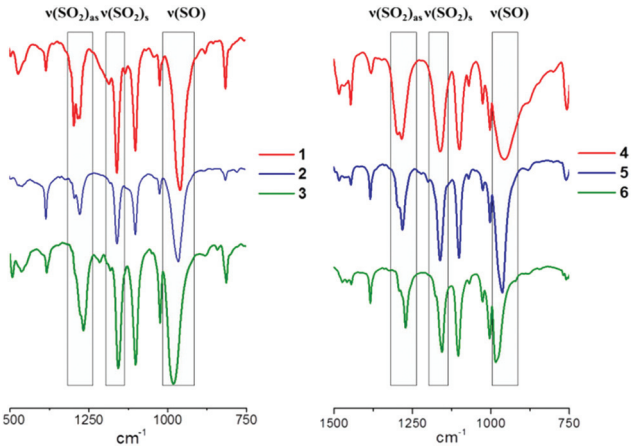

Fig. 2 The fingerprint regions in the FTIR spectra of **1–6**.

Redox properties

Oxidation and reduction of compounds **1–6** were investigated by cyclic voltammetry in acetonitrile and the results were compared with those obtained for the $(^n$Bu$_4$N$)_2[\{Mo_6X_8\}X_6]$ (X^- = Cl^-, Br^- and I^-) starting materials. Fig. 4S† shows the cyclic voltammograms of compounds **1–6**, while those of the starting materials are shown in Fig. 5S.† Table 1 summarises the most relevant data pertaining to the redox properties of the cluster complexes.

Oxidation of the starting complexes $(^n$Bu$_4$N$)_2[\{Mo_6X_8\}X_6]$ (X^- = Cl^-, Br^- and I^-) has been reported previously by Kirakci *et al.*[13] Our CV measurements confirmed the earlier data that $[\{Mo_6Cl_8\}Cl_6]^{2-}$ and $[\{Mo_6Br_8\}Br_6]^{2-}$ undergo one-electron reversible oxidation in the positive potential region, while $[\{Mo_6I_8\}I_6]^{2-}$ undergoes irreversible oxidation, with the oxidation potential lower than that for the lighter cluster anions (Table 1).[13]

CV measurements of compounds **1–3**, **5** and **6** showed quasi-reversible oxidation in the positive region at somewhat higher potentials than those observed for the corresponding $(^n$Bu$_4$N$)_2[\{Mo_6X_8\}X_6]$ complexes (Table 1). For compound **4** no oxidation peak was recorded up to a potential of 2 V. In summary it appears that substitution of the apical halide ligands by sulfonated aromatic ligands – benzenesulfonate and *p*-toluenesulfonate – increases the stability of the corresponding cluster complexes towards oxidation. Likewise, in analogous fashion to the starting complexes, oxidation of the complexes with heavier (iodide) cluster cores takes place at significantly lower potential, which signifies the noteworthy input of iodide ligand orbitals to the HOMO.

Similarly to earlier reported data on oxidation of octahedral molybdenum[13,46] and rhenium[47–49] cluster complexes, the

Table 1 Formal half-wave potentials ($E_{1/2}$), the peak current difference (ΔE_p) and the ratio of anodic and cathodic peak currents (I_{pa}/I_{pc}) for $[\{Mo_6X_8\}L_6]^{-/2-}$ couples, the potential of reduction (E_p^{red}), onset of oxidation (E_{ox}^{onset}) and reduction (E_{red}^{onset}) potentials and calculated electrochemical energy gaps of starting compounds $(Bu_4N)_2[\{Mo_6X_8\}X_6]$ (X^- = Cl^-, Br^- or I^-) and complexes **1–6** in acetonitrile *vs.* saturated Ag/AgCl couple: ΔE_p is the peak separation. The scan rate was 0.5 V s^{-1}. The optical energy gap is given for comparison

	$[Mo_6X_8L_6]^{2-} = [Mo_6X_8L_6]^- + e$			$[Mo_6X_8L_6]^{2-} + e$				
Compound	$E_{1/2}$, V	ΔE_p, mV	I_{pa}/I_{pc}	E_p^{red}, V	E_{ox}^{onset}, V	E_{red}^{onset}, V	Electrochemical energy gap, eV[a]	Optical energy gap, s eV
$(^nBu_4N)_2[\{Mo_6Cl_8\}Cl_6]$	1.78 (1.78[13])[b]	105	1.00	−1.40	1.70	−1.21	2.9	2.6
$(^nBu_4N)_2[\{Mo_6Br_8\}Br_6]$	1.55 (1.57[13])[b]	100	1.04	−1.35	1.51	−1.26	2.8	2.4 (2.4[52])
$(^nBu_4N)_2[\{Mo_6I_8\}I_6]$	1.02[c] (1.12[13])[b]	—	—	−1.25	0.70	−1.04	1.7	2.1
1	1.81	110	0.85	−1.09	1.72	−0.89	2.6	2.7
2	1.88	111	0.82	−1.14	1.77	−0.87	2.6	2.6
3	1.54	94	0.86	−1.13	1.44	−1.00	2.4	2.3
4	—	—	—	−1.15				2.7
5	1.93	97	0.85	−1.13	1.81	−0.81	2.6	2.4
6	1.54	170	0.89	−1.10	1.42	−0.81	2.2	2.2

[a] The electrochemical energy gap was estimated as a difference between E_{ox}^{onset} and E_{red}^{onset}. [b] Recalculated *vs.* saturated Ag/AgCl in acetonitrile. [c] The first oxidation peak current potential.

difference between anodic and cathodic potential peaks (ΔE_p) was higher than the "ideal" value of 59 mV in the Nernst equation for a one electron process. The increase of ΔE_p typically occurs because of uncompensated solution resistance and/or non-linear diffusion. Indeed, the anodic and cathodic peak currents, I_p(a) and I_p(c), respectively, were proportional to the square root of the scan rate, which agrees with Randles–Sevcik theory for processes controlled by diffusion. Moreover, the values of I_p(a)/I_p(c) for **1–3**, **5** and **6** indicate that some adsorption of the reactant could take place.[50]

In the negative potential region, both the starting compounds $(^nBu_4N)_2[\{Mo_6X_8\}X_6]$ (X^- = Cl^-, Br^- and I^-) and compounds **1–6** underwent irreversible reduction. Interestingly, the reduction of all compounds took place in a very narrow range of voltages ~−1.1 V (Table 1, Fig. 4S and 5S†). Such similarity in reduction potentials suggests that the LUMO orbital in the studied molybdenum complexes does not have significant input from the halide (inner) ligand orbitals. The irreversible nature of reduction is likely to be associated with the destruction of the cluster complexes, as it has been suggested previously for $[\{Mo_6Cl_8\}Cl_6]^{2-}$.[51]

It is known that cyclic voltammetry can be used to estimate the energy gap between the HOMO and the LUMO (also referred to as the electrochemical energy gap) as the difference between onsets of oxidation and reduction peaks. The values of the electrochemical band gap for the starting materials and the studied compounds decrease in the order Cl > Br > I for given apical ligands (Table 1).

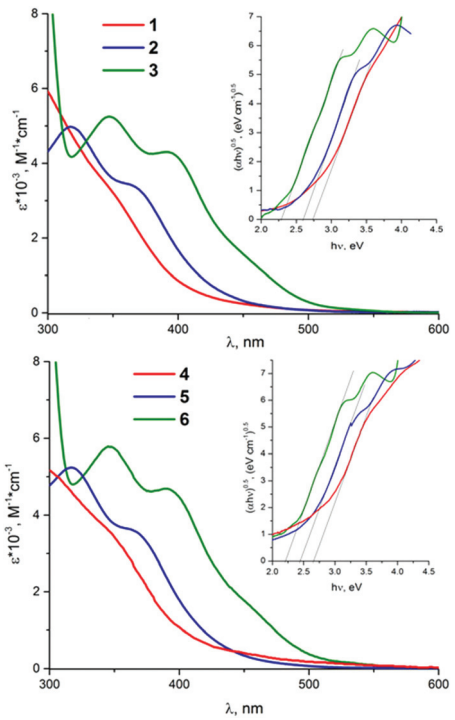

Fig. 3 The UV-vis spectra of **1–3** (top) and **4–6** (bottom) in dichloromethane. The inserts are the Tauc plots used to estimate excited state energy.

Absorption properties

The UV-vis absorption spectra of all the cluster complexes were recorded in dichloromethane and are shown in Fig. 3. Comparison of the absorption spectra of $(^nBu_4N)_2[\{Mo_6X_8\}X_6]$[13] with those of **1–6** shows that the substitution of apical halide ligands by sulfonate ones causes a blue shift of the absorption bands, especially in the case of the cluster complexes based on $\{Mo_6I_8\}^{4+}$ core. These observations further support the observation from electrochemical data about the significant input from the apical ligands in the HOMO. Taking into account the suggested nature of the HOMO and the LUMO, the lowest energy electronic transitions arise from ligand to metal charge transfer (LMCT). This is directly analogous to previously reported suggestions, based on theoretical calculations, for $[\{Mo_6X_8\}(NCS)_6]^{2-}$ (X^- = Cl^-, Br^-, I^-)[53] and isoelectronic rhenium clusters[54–56] with 24 valence electron counts (VEC).

UV-vis spectra of **1–6** show that the maxima of the absorptions as well as the values of the extinction coefficients do not depend on whether the apical ligand is benzenesulfonate or *p*-toluenesulfonate. A pronounced red shift of absorption band maxima is observed in the series Cl–Br–I. Similar bathochromic shifts of absorption maxima have been reported previously for $[\{Mo_6X_8\}X_6]^{2-}$, $[\{Mo_6X_8\}(NCS)_6]^{2-}$ (X = Cl^-, Br^-, I^-) and $[\{Mo_6X_8\}(CF_3COO)_6]^{2-}$.[13,57,58] These shifts signify that the energy gap between the HOMO and the LUMO in cluster complexes $[\{Mo_6X_8\}L_6]^{2-}$ decreases in the order Cl > Br > I for given apical ligands. This order was further confirmed, when the energy gaps (also known as the optical energy gap) were estimated *via* Tauc plot (see inserts in Fig. 3 as well as Fig. 6S†). These optical energy gaps, obviously, refer to spin-allowed (*i.e.* singlet state to singlet state) transitions. The above values for the electrochemical band gap for the starting materials and the studied compounds are comparable with the optical energy band gaps found from absorption spectra (Table 1). Moreover the same trend in terms of the widths of the energy gaps is also observed, *i.e.* the optical energy gap decreases in the order Cl > Br > I for given apical ligands.

Photoluminescence properties

The normalised photoluminescence spectra of samples **1–6** in the solid state and in deaerated acetonitrile solutions are shown in Fig. 4. The photophysical characteristics, namely emission maximum wavelengths (λ_{em}), quantum yields (Φ_{em}) and lifetimes (τ_{em}) with the corresponding amplitudes (A), of all samples measured in the solid state as well as in air-equilibrated and deaerated acetonitrile solutions are summarised in Table 2.

As Table 2 shows, the photophysical characteristics of the complexes are strongly dependent on the halide ligand in the cluster core and only slightly on the composition of the apical ligands.

Generally, all of the complexes, in both the solid state and in acetonitrile solution, exhibited red photoluminescence with broad spectral emission profiles ranging from ~550 to longer than 900 nm. These are typical photoluminescence emission profiles for compounds based on $\{Mo_6X_8\}^{4+}$ (X^- = Cl^-, Br^- or I^-) cluster cores.[9–15,38] Notably, the emission profiles of iodide complexes **3** and **6** are significantly narrower and blue shifted compared with the emission profiles of the chloride and bromide-containing clusters. In combination absorption and photoluminescence spectra of **1–6** show that the emission in the case of $\{Mo_6I_8\}^{4+}$ occurs mostly from the triplet state that is closer to the excited singlet state than that in the case of $\{Mo_6Cl_8\}^{4+}$ and $\{Mo_6Br_8\}^{4+}$. This intriguing feature of $[\{Mo_6I_8\}L_6]^{2-}$ cluster complexes, where L is a residue oxygenated acid has been noticed earlier by us and other groups.[9–11,13,38]

The solid state luminescence properties of complexes **1–6** are highly encouraging being characterised by quantum yields, from 0.13 to 0.62. The highest quantum yields were found for complexes **3** and **6**, *i.e.* those comprising the $\{Mo_6I_8\}^{4+}$ cluster core. The luminescence lifetimes of all the solid samples were

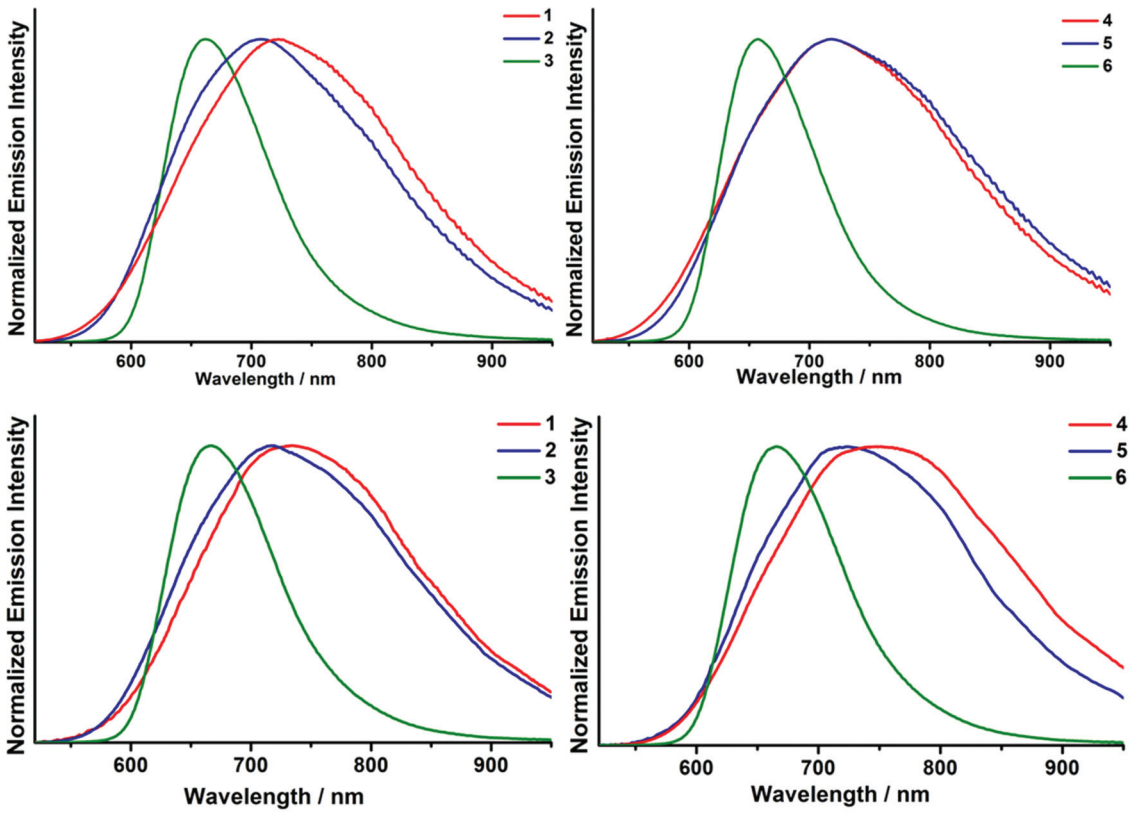

Fig. 4 Normalised emission spectra of **1–6** in the solid state (top) and in deaerated acetonitrile solutions (bottom).

Table 2 Spectroscopic and photophysical parameters of cluster complexes **1–6** determined for powdered samples and both aerated (non-degassed) and deaerated CH_3CN solutions. λ_{em} is an emission maximum wavelength; fwhm is the value of full width at half maximum of the emission spectrum; τ_{em} are the photoluminescence lifetimes with the corresponding amplitudes (A) for the photoluminescence decay equation, where intensity (I) of photoluminescence vs time is expressed as $I = I_0 \sum_{i=1}^{n} A_i \exp\left(-\frac{t}{\tau_i}\right)$; Φ_{em} is photoluminescence quantum yield

		$(^nBu_4N)_2[\{Mo_6X_8\}(OTs)_6]$			$(^nBu_4N)_2[\{Mo_6X_8\}(C_6H_5SO_3)_6]$		
		λ_{em}, nm (fwhm, cm^{-1})	τ_{em}, μs (A)	Φ_{em}	λ_{em}, nm (fwhm, cm^{-1})	τ_{em}, μs	Φ_{em}
X = Cl	Powdered sample	723 (~4000)	τ_1 = 228 (0.7) τ_2 = 174 (0.3)	0.34	719 (~4200)	τ_1 = 127 (0.3) τ_2 = 75 (0.7)	0.13
	Aerated solution	735 (~3850)	τ_1 = 5.1 (0.3) τ_2 = 1.2 (0.7)	<0.01	723 (~4050)	τ_1 = 3.9 (0.4) τ_2 = 0.5 (0.6)	<0.01
	Deaerated CH_3CN solution	735 (~3850)	τ_1 = 9.8 (0.2) τ_2 = 3.0 (0.8)	<0.01	723 (~4050)	τ_1 = 9.2 (0.1) τ_2 = 2.6 (0.9)	<0.01
X = Br	Powdered sample	708 (~4100)	τ_1 = 185 (0.7) τ_2 = 86 (0.3)	0.29	718 (~4350)	τ_1 = 124 (0.3) τ_2 = 52 (0.7)	0.13
	Aerated CH_3CN solution	717 (~4150)	15	<0.01	750 (~4150)	13	<0.01
	Deaerated CH_3CN solution	717 (~4150)	243	0.26	750 (~4150)	179	0.17
X = I	Powdered sample	662 (~2300)	τ_1 = 135 (0.6) τ_2 = 56 (0.4)	0.44	657 (~2200)	τ_1 = 183 (0.6) τ_2 = 57 (0.4)	0.62
	Aerated CH_3CN solution	667 (~2400)	5.0	0.01	665 (~2400)	5.2	0.01
	Deaerated CH_3CN solution	667 (~2400)	305	0.65	665 (~2400)	263	0.60

fitted by double exponential decays that are usually explained by an efficient excitation energy migration and subsequent energy trap/emission in the crystalline phase.

The emission spectra for each compound, in both aerated and deaerated solutions, have almost identical profiles. For solutions of the bromide and iodide complexes (**2**, **3**, **5** and **6**) the deaerated solutions are characterised by significantly higher quantum yields and longer lifetimes than those observed for the corresponding aerated systems (Table 2). This difference may be explained readily by the fact that the long-lived luminescence of hexanuclear cluster complexes is well known to be quenched efficiently by oxygen.[9–11,38]

Chloride complexes **1** and **4** behaved differently from their bromide and iodide analogues. Even in a deaerated acetonitrile solution these complexes demonstrated very weak and relatively short-lived luminescence despite the relatively high τ_{em} and Φ_{em} values found for them in the solid state (Table 2). Similar low levels of luminescence in solution with a double exponential emission decay and relatively small lifetimes have also been reported previously for $\{Mo_6Cl_8\}^{4+}$-based clusters coordinated by fluorinated carboxylate apical ligands.[9,13]

In contrast, as in our work, the emissions of dissolved related bromide, and especially, iodide clusters were characterised by very high emission quantum yields with decay profiles fitted well by single exponential functions and τ_{em} values of hundreds of microseconds.[9,13] Since oxygen quenches the luminescent emissions of cluster complexes **1–6** effectively (Table 4S†), we were keen to explore the potential of these materials in applications associated with the use of singlet oxygen generated *in situ*. Therefore, we compared the ability of each of the cluster complexes **1–6** to generate singlet oxygen using a semi-quantitative test based on oxidation of the singlet oxygen trap molecule, 2,3-diphenyl-*p*-dioxene.

Accordingly, ^{1}H NMR was used to trace oxidation of 2,3-diphenyl-*p*-dioxene in the presence of the cluster complexes. Specifically, 1 : 100 molar mixtures of each cluster complex : trap were irradiated for periods of 1, 3 and 5 h. The results obtained unambiguously confirmed the successful generation of singlet oxygen by all six complexes **1–6** (Fig. 5, 1S and 2S,

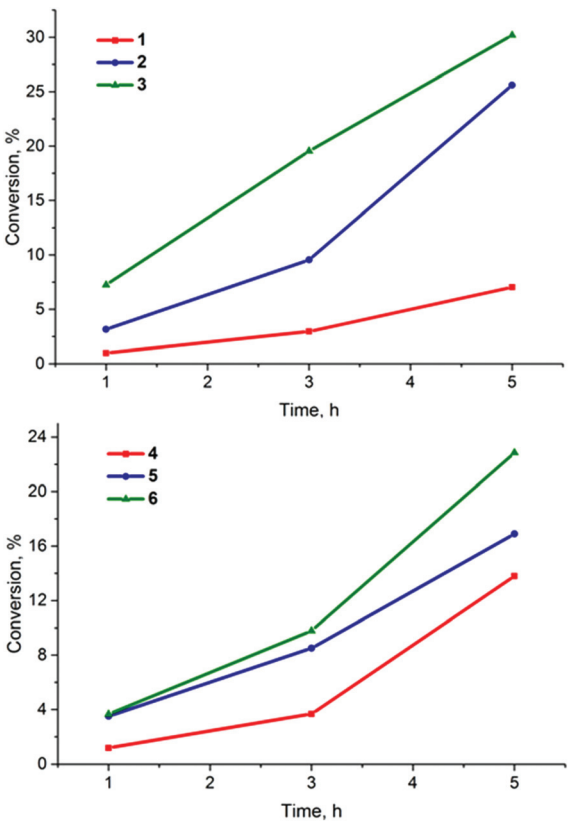

Fig. 5 The conversion of 2,3-diphenyl-*p*-dioxene into ethylene glycol dibenzoate in the presence of **1–6** after photoirradiation with $\lambda \geq 400$ nm.

Table 4S†). The rate of oxidation of the 2,3-diphenyl-*p*-dioxene was dependent on the halide ligand present in the cluster core and decreased in the order I > Br > Cl for given apical ligands. This order of singlet oxygen generation efficiencies correlates well with the photoluminescence quantum yields recorded in deaerated acetonitrile solutions of **1–6**.

Conclusions

In this work we synthesised and characterised, in detail, octahedral molybdenum cluster complexes, where the cores $\{Mo_6X_8\}^{4+}$ (X^- = Cl^-, Br^- or I^-) are coordinated by aromatic sulfonates – either *p*-toluenesulfonate or benzenesulfonate. Our study clearly confirms the strong effect that the inner halide ligands exert on the photophysical and redox properties of the obtained cluster complexes. Specifically UV-vis and CV studies showed that the energy gap between ground state and the first singlet (exited) state decreases in the order Cl > Br > I, while the gap between emissive (triplet) state and the ground state increases in the same order. Furthermore, our data also suggest that the HOMO orbital has a significant input from halide ligands, especially in the case of iodide cluster complexes, while the LUMO is predominantly Mo_6 derived in nature.

All of the cluster complexes displayed strong red luminescence in the solid state, while only those with heavier cluster cores (*i.e.* Br^- and I^- inner ligands) showed outstanding photoluminescence in deaerated acetonitrile solutions. Notably, cluster complexes with $\{Mo_6I_8\}^{4+}$ cores showed the highest quantum yields and the narrowest and most strongly blue-shifted emission spectra. Moreover, $[\{Mo_6I_8\}(OTs)_6]^{2-}$ and $[\{Mo_6I_8\}(PhSO_3)_6]^{2-}$ also showed the highest singlet oxygen generation efficiency in comparison with the chloride and bromide analogues. This study thus further suggests that synthesis of highly photoactive compounds and materials may be generally achieved by coordinating of octahedral cluster $\{Mo_6I_8\}^{4+}$ by residues of strong oxoacids. In order to facilitate the rational design of materials with bespoke photophysical properties, detailed study should be undertaken to uncover whether there is any dependence between the acidy of an oxoacid and the photoluminescence parameters of the corresponding octahedral molybdenum cluster complexes.

Acknowledgements

This work was supported by a Marie-Curie Intra-European Fellowship (No. 327440), by the Russian Foundation for Basic Research (Grant No. 14-03-92612), the Royal Society (IE140281) and by the Grant of the President of the Russian Federation (MK 4054.2015.3). K. A. Brylev thanks the Japan Society for the Promotion of Science (JSPS) for a post-doctoral fellowship for foreign researchers.

References

1 J. C. Sheldon, *Nature*, 1959, **184**, 1210–1213.
2 J. C. Sheldon, *J. Chem. Soc.*, 1960, 1007–1014.
3 J. C. Sheldon, *Chem. Ind.*, 1961, 323.
4 J. C. Sheldon, *J. Chem. Soc.*, 1963, 4183–4186.
5 A. W. Maverick and H. B. Gray, *J. Am. Chem. Soc.*, 1981, **103**, 1298–1300.
6 A. W. Maverick, J. S. Najdzionek, D. MacKenzie, D. G. Nocera and H. B. Gray, *J. Am. Chem. Soc.*, 1983, **105**, 1878–1882.
7 D. G. Nocera and H. B. Gray, *J. Am. Chem. Soc.*, 1984, **106**, 824–825.
8 Y. Saito, H. K. Tanaka, Y. Sasaki and T. Azum, *J. Phys. Chem.*, 1985, **89**, 4413–4415.
9 M. N. Sokolov, M. A. Mihailov, E. V. Peresypkina, K. A. Brylev, N. Kitamura and V. P. Fedin, *Dalton Trans.*, 2011, **40**, 6375–6377.
10 M. N. Sokolov, M. A. Mikhailov, K. A. Brylev, A. V. Virovets, C. Vicent, N. B. Kompankov, N. Kitamura and V. P. Fedin, *Inorg. Chem.*, 2013, **52**, 12477–12481.
11 O. A. Efremova, M. A. Shestopalov, N. A. Chirtsova, A. I. Smolentsev, Y. V. Mironov, N. Kitamura, K. A. Brylev and A. J. Sutherland, *Dalton Trans.*, 2014, **43**, 6021–6025.
12 K. Kirakci, K. Fejfarova, M. Kucerakova and K. Lang, *Eur. J. Inorg. Chem.*, 2014, 2331–2336.
13 K. Kirakci, P. Kubat, J. Langmaier, T. Polivka, M. Fuciman, K. Fejfarova and K. Lang, *Dalton Trans.*, 2013, **42**, 7224–7232.
14 K. Kirakci, P. Kubat, M. Dusek, K. Fejfarova, V. Sicha, J. Mosinger and K. Lang, *Eur. J. Inorg. Chem.*, 2012, 3107–3111.
15 K. Kirakci, V. Sicha, P. Holub and K. Lang, *Inorg. Chem.*, 2014, **53**, 13012–13018.
16 J. A. Jackson, M. D. Newsham, C. Worsham and D. G. Nocera, *Chem. Mater.*, 1996, **8**, 558–564.
17 S. Chenais and S. Forget, *Polym. Int.*, 2011, **61**, 390–406.
18 H. Liu, J. B. Edel, L. M. Bellan and H. G. Craighead, *Small*, 2006, **2**, 495–499.
19 B. C. Rowan, L. R. Wilson and B. S. Richards, *IEEE J. Sel. Top. Quantum Electron.*, 2008, **14**, 1312–1322.
20 C. Vonesch, F. Aguet, J.-L. Vonesch and M. Unser, *IEEE Signal Process. Mag.*, 2006, 20–31.
21 J. F. Lovell, T. W. B. Liu, J. Chen and G. Zheng, *Chem. Rev.*, 2010, **110**, 2839–2857.
22 F. Vatansever, W. C. M. A. de Melo, P. Avci, D. Vecchio, M. Sadasivam, A. Gupta, R. Chandran, M. Karimi, N. A. Parizotto, R. Yin, G. P. Tegos and M. R. Hamblin, *Microbiol. Rev.*, 2013, **37**, 955–989.
23 D. E. J. G. J. Dolmans, D. Fukumura and R. K. Jain, *Nat. Rev. Cancer*, 2003, **3**, 380–387.
24 P. Agostinis, K. Berg, K. A. Cengel, H. Foster, A. W. Girotti, S. O. Gollnick, S. M. Hahn, M. R. Hamblin, A. Juzeniene, D. Kessel, M. Korbelik, J. Moan, P. Mroz, D. Nowis, J. Piette, B. C. Wilson and J. Golab, *CA-Cancer J. Clin.*, 2011, **61**, 250–281.
25 M. C. DeRosa and R. J. Crutchley, *Coord. Chem. Rev.*, 2002, **233–234**, 351–371.
26 A. Barras, S. Cordier and R. Boukherroub, *Appl. Catal., B*, 2012, **123–124**, 1–8.

27 A. O. Solovieva, Y. A. Vorotnikov, K. E. Trifonova, O. A. Efremova, A. A. Krasilnikova, K. A. Brylev, E. V. Vorontsova, P. A. Avrorov, L. V. Shestopalova, A. F. Poveshchenko, Y. V. Mironov and M. A. Shestopalov, *J. Mater. Chem. B*, 2016, **4**, 4839–4846.
28 A. Flemström, T. K. Hirsch, L. Eriksson and S. Lidin, *Solid State Sci.*, 2004, **6**, 509–517.
29 K. Kirakci, S. Cordier and C. Perrin, *Z. Anorg. Allg. Chem.*, 2005, **631**, 411–416.
30 W. Preetz and K. Harder, *J. Alloys Compd.*, 1992, **183**, 413–429.
31 P. Bruckner, W. Preetz and M. Punjer, *Z. Anorg. Allg. Chem.*, 1997, **623**, 8–17.
32 K. Kirakci, S. Cordier, T. Roisnel, S. Golhen and C. Perrin, *Z. Kristallogr. - New Cryst. Struct.*, 2005, **220**, 116–118.
33 A. P. Cote and G. K. H. Shimizu, *Inorg. Chem.*, 2004, **43**, 6663–6676.
34 R. K. Summerbell and D. R. Berger, *J. Am. Chem. Soc.*, 1959, **81**, 633–639.
35 *Bruker, APEX2 (Version 1.08), SAINT (Version 7.03), SADABS (Version 2.11), SHELXTL (Version 6.12)*, Bruker AXS Inc., Madison, WI, USA, 2004.
36 L. Gao, M. A. Peay and T. G. Gray, *Chem. Mater.*, 2010, **22**, 6240–6245.
37 M. A. Shestopalov, K. E. Zubareva, O. P. Khripko, Y. I. Khripko, A. O. Solovieva, N. V. Kuratieva, Y. V. Mironov, N. Kitamura, V. E. Fedorov and K. A. Brylev, *Inorg. Chem.*, 2014, **53**, 9006–9013.
38 M. A. Mikhailov, K. A. Brylev, A. V. Virovets, M. R. Gallyamov, I. N. Novozhilov and M. N. Sokolov, *New J. Chem.*, 2016, **40**, 1162–1168.
39 D. H. Johnston, D. C. Gaswick, M. C. Lonergan, C. L. Stern and D. F. Shriver, *Inorg. Chem.*, 1992, **31**, 1869–1873.
40 P. Braack, M. K. Simsek and W. Preetz, *Z. Anorg. Allg. Chem.*, 1998, **624**, 375–380.
41 M. N. Sokolov, M. A. Mihailov, P. A. Abramov and V. P. Fedin, *J. Struct. Chem.*, 2012, **53**, 197–201.
42 M. N. Sokolov, M. A. Mikhailov, A. V. Virovets, K. A. Brylev, R. A. Bredikhin, A. M. Maksimov, V. E. Platonov and V. P. Fedin, *Russ. Chem. Bull.*, 2013, **62**, 1764–1767.
43 C. R. Groom, I. J. Bruno, M. P. Lightfoot and S. C. Ward, *Acta Crystallogr., Sect. B: Struct. Sci.*, 2016, **72**, 171–179.
44 S. Detoni and D. Hadzi, *Spectrochim. Acta*, 1956, **11**, 601–608.
45 S. M. Holmes, S. G. Mckinley and G. S. Girolami, *Inorg. Synth.*, 2002, **33**, 91–93.
46 K. Kirakci, S. Cordier, O. Hernandez, T. Roisnel, F. Paul and C. Perrin, *J. Solid State Chem.*, 2005, **178**, 3117–3129.
47 T. Yoshimura, K. Umakoshi, Y. Sasaki, S. Ishizaka, H. B. Kim and N. Kitamura, *Inorg. Chem.*, 2000, **39**, 1765–1772.
48 Y. Molard, A. Ledneva, M. Amela-Cortes, V. Circu, N. G. Naumov, C. Meriadec, F. Artzner and S. Cordier, *Chem. Mater.*, 2011, **23**, 5122–5130.
49 Z. P. Zheng, T. G. Gray and R. H. Holm, *Inorg. Chem.*, 1999, **38**, 4888–4895.
50 R. H. Wopschall and I. Shain, *Anal. Chem.*, 1967, **39**, 1514–1527.
51 P. A. Barnard, I.-W. Sun and C. L. Hussey, *Inorg. Chem.*, 1990, **29**, 3670–3674.
52 P. Kumar, S. Kumar, S. Cordier, S. Paofai, R. Boukherroub and S. L. Jain, *RSC Adv.*, 2014, **4**, 10420–10423.
53 R. Ramirez-Tagle and R. Arratia-Perez, *Chem. Phys. Lett.*, 2008, **460**, 438–441.
54 R. Arratia-Perez and L. Hernandez-Acevedo, *J. Chem. Phys.*, 1999, **111**, 168–172.
55 R. Arratia-Perez and L. Hernandez-Acevedo, *J. Chem. Phys.*, 1999, **110**, 2529–2532.
56 L. Hernandez-Acevedo and R. Arratia-Perez, *J. Chil. Chem. Soc.*, 2003, **48**, 125–128.
57 R. Rramirez-Tagle and R. Arratia-Perez, *Chem. Phys. Lett.*, 2008, **460**, 438–441.
58 R. Rramirez-Tagle and R. Arratia-Perez, *Chem. Phys. Lett.*, 2008, **455**, 38–41.